ELSEVIER

Earth and Planetary Science Letters 187 (2001) 367–379

EPSL

www.elsevier.com/locate/epsl

Numerical models of the onset of yield strength in crystal–melt suspensions

Martin O. Saar *, Michael Manga, Katharine V. Cashman, Sean Fremouw

Department of Geological Sciences, University of Oregon, Eugene, OR 97403, USA

Received 15 November 2000; received in revised form 15 February 2001; accepted 19 February 2001

Abstract

The formation of a continuous crystal network in magmas and lavas can provide finite yield strength, τ_y, and can thus cause a change from Newtonian to Bingham rheology. The rheology of crystal–melt suspensions affects geological processes, such as ascent of magma through volcanic conduits, flow of lava across the Earth's surface, melt extraction from crystal mushes under compression, convection in magmatic bodies, and shear wave propagation through partial melting zones. Here, three-dimensional numerical models are used to investigate the onset of 'static' yield strength in a zero-shear environment. Crystals are positioned randomly in space and can be approximated as convex polyhedra of any shape, size and orientation. We determine the critical crystal volume fraction, ϕ_c, at which a crystal network first forms. The value of ϕ_c is a function of object shape and orientation distribution, and decreases with increasing randomness in object orientation and increasing shape anisotropy. For example, while parallel-aligned convex objects yield $\phi_c = 0.29$, randomly oriented cubes exhibit a maximum ϕ_c of 0.22. Approximations of plagioclase crystals as randomly oriented elongated and flattened prisms (tablets) with aspect ratios between 1:4:16 and 1:1:2 yield $0.08 < \phi_c < 0.20$, respectively. The dependence of ϕ_c on particle orientation implies that the flow regime and resulting particle ordering may affect the onset of yield strength. ϕ_c in zero-shear environments is a lower bound for ϕ_c. Finally the average total excluded volume is used, within its limitation of being a 'quasi-invariant', to develop a scaling relation between τ_y and ϕ for suspensions of different particle shapes.

Keywords: yield strength; crystals; lava flows; flow mechanism; rheology; magmas

1. Introduction

Magmas and lavas typically contain crystals, and often bubbles, suspended in a liquid. These crystal–melt suspensions vary considerably in crystal volume fraction, ϕ, and range from crystal-free in some volcanic eruptions, to melt-free in portions of the Earth's mantle. Moreover, the concentration of suspended crystals often changes with time due to cooling or degassing, which causes crystallization, or due to heating, adiabatic decompression, or hydration, which causes melting. Such variations in ϕ can cause continuous or abrupt modifications in rheological properties such as yield strength, viscosity, and fluid–solid transitions. Thus, the mechanical properties of geologic materials vary as a result of the large

* Corresponding author. Fax: +1-541-346-4692; E-mail: martin@newberry.uoregon.edu

0012-821X/01/$ – see front matter
PII: S0012-821X(01)00289-8

range of crystal fractions present in geologic systems. The rheology of crystal–melt suspensions affects geological processes, such as ascent of magma through volcanic conduits, flow of lava across the Earth's surface, convection in magmatic reservoirs, and shear wave propagation through zones of partial melting.

One example of a change in rheological properties that may influence a number of magmatic processes is the onset of yield strength in a suspension once ϕ exceeds some critical value, ϕ_c. The onset of yield strength has been proposed as a possible cause for morphological transitions in surface textures of basaltic lava flows [1]. Yield strength development may also be a necessary condition for melt extraction from crystal mushes under compression, for example in flood basalts or in the partial melting zone beneath mid-ocean ridges [2]. Furthermore, an increase of viscosity and development of yield strength in magmatic suspensions may cause volcanic conduit plug formation and the transition from effusive to explosive volcanism [3]. Indeed, Philpotts et al. [2] state that the development of a load-bearing crystalline network is "one of the most important steps in the solidification of magma".

In this paper we employ three-dimensional (3D) numerical models of crystal–melt suspensions to investigate the onset of yield strength, τ_y. Yield strength development due to vesicles [4,5] is not considered in this study. The objective is to understand the geometrical properties of the crystals in suspension that determine the critical crystal volume fraction, ϕ_c, at which a crystal network first forms. Our simulations suggest that the onset of yield strength in crystal–melt suspensions may occur at crystal fractions that are lower than the 0.35–0.5 commonly assumed [6–8] in static (zero-shear) environments. We demonstrate that yield strength can develop at significantly lower ϕ when crystals have high shape anisotropy and are randomly oriented, and that an upper bound should be given by $\phi_c = 0.29$ for parallel-aligned objects. Because particle orientation is a function of the stress tensor, we expect increasing particle alignment with increasing shear stress and perfect alignment in pure shear only [9]. Furthermore, we suggest a scaling relation between τ_y and ϕ for suspensions of different particle shapes. Our numerical models complement the experimental studies presented in a companion paper [10].

2. Rheology of magmatic suspensions

In this section we provide an overview of the conceptual framework in which we interpret our results. Fig. 1 illustrates schematically the relationship between effective shear viscosity, μ_{eff}, yield strength, τ_y, and particle volume fraction, ϕ. We make a distinction between fluid and solid (regions A and B, respectively, in Fig. 1). The subcategories A' and A'' are used for suspensions with $\tau_y = 0$ (Newtonian) and $\tau_y > 0$ (Bingham), respectively. We assume here that the suspensions are not influenced by non-hydrodynamic (e.g. colloidal) forces, Brownian motion, or bubbles. First we discuss viscosity (region A) then yield strength (subregion A'').

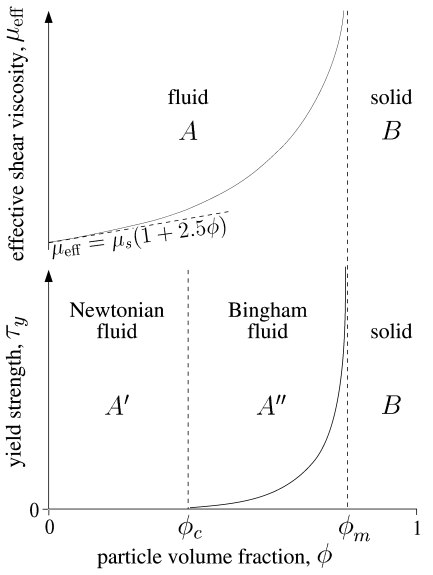

Fig. 1. Sketch of the development of effective shear viscosity, μ_{eff}, and yield strength, τ_y, as a function of crystal fraction, ϕ. The critical crystal fractions ϕ_c and ϕ_m depend on the total shear stress, τ, and particle attributes, ξ, such as particle shape, size, and orientation distribution. A first minimum yield strength develops at $\phi_c \equiv \phi_c(\xi, \tau_y = 0)$ and increases with increasing ϕ. The fields A, A', A'', and B are explained in the text.

2.1. Fluid behavior: region A

Einstein [11] found an analytical solution, $\mu_{eff} = \mu_s(1+2.5\phi)$, describing the effective shear viscosity, μ_{eff}, of a dilute ($\phi \leq 0.03$) suspension (left hand side of field A) of spheres for very low Reynolds numbers (Stokes flow). The viscosity of the suspending liquid is μ_s. The particle concentration, ϕ, has to be sufficiently low that hydrodynamic interactions of the particles can be neglected.

At higher ϕ (right hand side of field A) the so-called Einstein–Roscoe equation [12–14] is often employed to incorporate effects of hydrodynamically interacting, non-colloidal particles:

$$\mu_r = \mu_{eff}/\mu_s = (1-\phi/\phi_m)^{-2.5} \quad (1)$$

where ϕ_m is the maximum packing fraction. The form of Eq. 1 allows the relative viscosity μ_r to diverge as $\phi \rightarrow \phi_m$. Eq. 1 is commonly used to calculate the viscosity of magmas [7]. However, the value of ϕ_m, which determines the transition to a solid, is uncertain; suggested values range from $\phi_m = 0.74$ [13] to $\phi_m = 0.60$ [15]. $\phi_m = 0.74$ corresponds to the maximum packing fraction of uniform spheres, so ϕ_m might be expected to be different if non-spherical particles are considered [7,15]. An additional complication is the tendency of crystals to form aggregates or networks. Jeffrey and Acrivos [14] argue that a suspension that forms aggregates can be viewed as a suspension of single particles of new shapes (and sizes) and thus possessing different rheological properties.

2.2. Onset and development of yield strength: region A″

Suspensions may have a range of yield strengths τ_y (subregion A'') [16]. At ϕ_c a first sample-spanning crystal network forms to provide some minimum yield strength ($\tau_y \rightarrow 0$). For $\phi \geq \phi_c$ yield strength increases with increasing ϕ. The fluid–solid transition occurs at the maximum packing fraction, ϕ_m.

In general we expect ϕ_c and ϕ_m to depend on particle attributes (denoted ξ), such as particle shape, size, and orientation distribution, as well as on total applied stress, τ, e.g. $\phi_m = \phi_m(\xi, \tau)$. The dependence of ϕ_c and ϕ_m on τ results from hydrodynamic forces that can break and orient the crystal network and transform it into a more ordered state of denser packing. Here we define $\phi_c \equiv \phi_c(\xi, \tau = 0)$. As τ_y approaches zero, the minimum critical crystal fraction, ϕ_c, is obtained for a given ξ. The development of yield strength, τ_y, may thus be described by:

$$\tau_y(\phi) = [(\phi/\phi_c - 1)/(1-\phi/\phi_m)]^{1/p}\tau_{co} \quad (2)$$

where τ_{co} reflects the total interparticulate cohesion resisting hydrodynamic forces and p may reflect the response of the aggregate state to shearing [16–18].

In this study we investigate the influence of ξ on ϕ_c as $\tau \rightarrow 0$, with the implication that the onset of zero-shear yield strength is a lower bound for the onset of yield strength in shear environments. Thus, ϕ_c may be viewed as the lowest crystal volume fraction at which τ_y could possibly form under the given assumptions (e.g. no non-hydrodynamic forces, bubbles, or Brownian motion).

3. Methods

In contrast to natural and analog experiments, computer models permit investigation of the formation of a continuous crystal network at low ϕ under static conditions (zero strain rate). As experimental and in situ measurements of yield strength may disrupt the fragile network that first forms at ϕ_c, it has been argued [6,19] that incorrect extrapolation of stress versus strain rate measurements towards zero strain rate can lead to fictitious yield strength values when in actuality the suspension is shear-thinning. Moreover, simulations allow the intergrowth of crystals, which is important for systems where the crystal growth rate, G, is significantly larger than the shear rate, $\dot{\gamma}$, as is the case in some natural systems [2,20]. In this study we assume a zero-shear environment, thus:

$$\frac{\dot{\gamma}}{G} \rightarrow 0 \quad (3)$$

We employ continuum percolation models to study the possible development of τ_y as a function of ϕ and ξ. Percolation theory describes the interconnectivity of individual elements in disordered (random) systems and suggests a power law relationship of the form [21]:

$$\tau_y \sim \begin{cases} 0 & \phi < \phi_c \\ (\phi - \phi_c)^{\eta} & \phi \geq \phi_c \end{cases} \quad (4)$$

where ϕ_c is the percolation threshold which is reached when crystals first form a continuous phase across the suspending fluid. The exponent η describes the development of τ_y for $\phi \geq \phi_c$ close to ϕ_c. Although phenomenological, we determine a geometrical percolation threshold, p_c, and assume that it is related to ϕ_c [22]. With this approach, we can investigate the dependence of p_c on crystal shape, size, and orientation distribution and draw conclusions about the effects of these geometric properties on the development of yield strength.

The crystals in our simulations can be approximated as convex polyhedra of any shape, size, and orientation distribution in 3D space. Crystals are positioned randomly and interpenetrate each other (soft-core continuum percolation). In soft-core percolation the concept of maximum packing fraction, ϕ_m, does not apply. Fig. 2a shows that

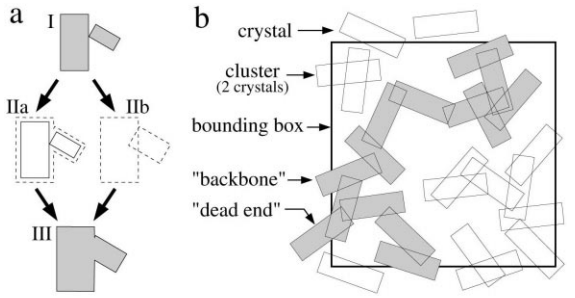

Fig. 2. (a) Simulation of crystal intergrowth. (I) Crystals touch; (IIa) in natural systems under high growth rate to shear rate ratios, touching crystals grow together; (IIb) in the computer model crystals overlap; (III) same end result. (b) Schematic 2D illustration of crystals forming clusters. One cluster connects opposite sides of the bounding box and forms the backbone. It is necessary that some crystals are positioned outside the bounding box, so that they can protrude into it. Actual simulations are 3D (Fig. 4).

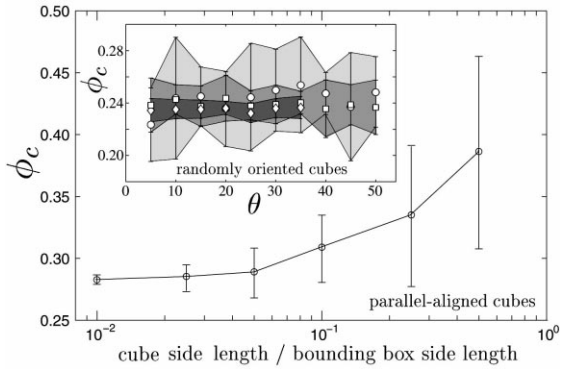

Fig. 3. Critical crystal volume fraction, ϕ_c, versus ratio of cube side length, l_c, over bounding box side length, $l_b = 1$, for parallel-aligned cubes. Inset: ϕ_c versus number of resolution grains, θ, per distance from the crystal center to the farthest vertex, d, for randomly oriented cubes. Symbols are the mean and shaded areas indicate standard deviations. Circle (light gray area): $l_c/l_b = 0.1$; square (medium gray area): $l_c/l_b = 0.05$; diamond (dark gray area): $l_c/l_b = 0.025$. The total number of grains is $\theta_t \approx (\theta/d)^3$, where for a cube $d = (3l_c^2)^{1/2}$.

overlapping crystals of a finite size may simulate crystal intergrowth in a zero-shear environment. Crystal orientation distribution is pre-assigned so that, for example, parallel-aligned or randomly oriented distributions can be simulated. Crystals are positioned inside and outside a bounding unit cube (Fig. 2b). To avoid finite size effects, the maximum length of the largest crystal in a given simulation is never longer than 1/10, and typically 1/20 to 1/40, of the bounding cube side length. Fig. 3 shows the decrease in standard deviation and mean of ϕ_c for decreasing particle side length for parallel-aligned cubes.

We determine crystal overlaps analytically. Volume fractions, ϕ, are determined numerically by discretizing the bounding cube into subcubes (grains). The inset of Fig. 3 illustrates that while crystal size influences the standard deviation of ϕ_c (gray shaded areas), 'grain resolution', θ, is relatively uncritical for calculations of ϕ. This insensitivity could be due to the angular crystal shapes that may be approximated well by a few angular grains. We also determine ϕ by using the number of crystals per unit volume, n, and the volume of a crystal, v, in $\phi = 1 - \exp(-nv)$ [23,24].

Crystals that overlap are part of a 'cluster'. Overlapping crystals of different clusters cause

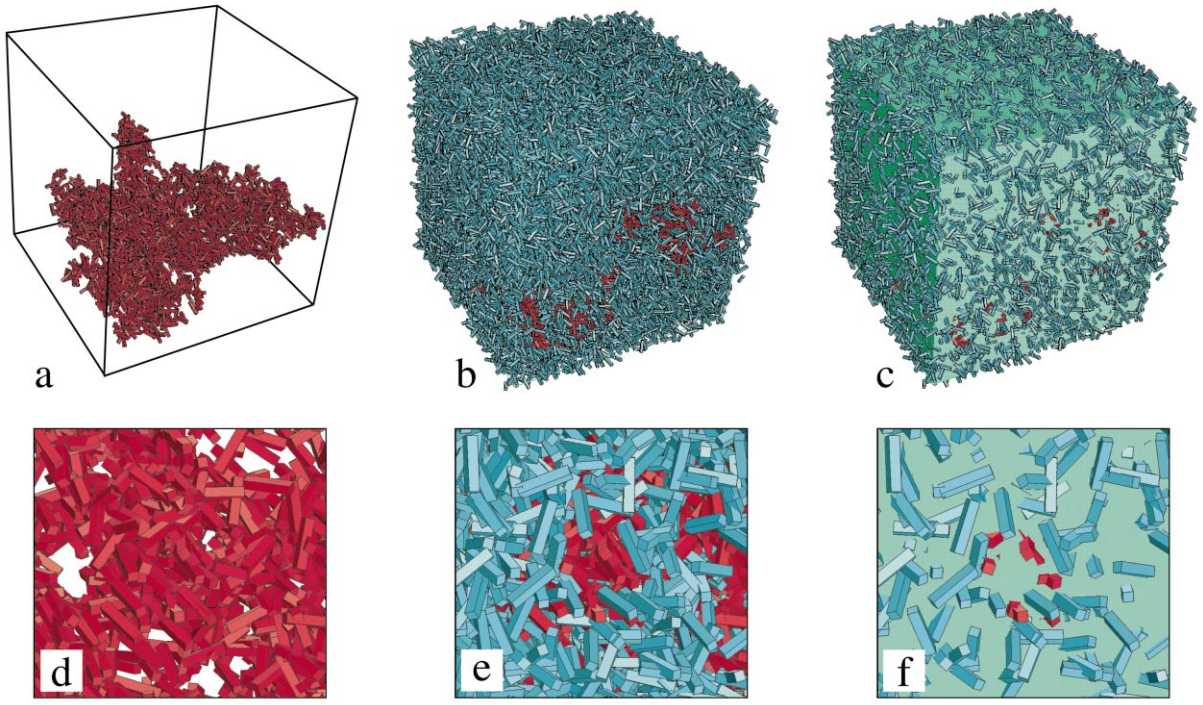

Fig. 4. Visualizations of a simulation of randomly oriented elongated rectangular biaxial soft-core prisms of aspect ratio 5:1, at the percolation threshold; (a) only backbone crystals, connecting four of the six cube faces, (b) all crystals, (c) all crystals that protrude out of the bounding cube. (d), (e), and (f) are magnifications of a region in (a), (b), and (c), respectively. The total crystal volume fraction in this simulation is $\phi_c = 0.132$ (backbone volume fraction: 0.016). The total number of crystals is 28 373 of which 3400 are part of the backbone.

the two clusters to merge into one. The percolation threshold is reached when a continuous crystal chain (hereafter referred to as the 'backbone') exists, connecting one face of the bounding cube with the opposing face (Figs. 2b and 4a). A backbone in this study includes the 'dead-end branches' which may not be considered part of the backbone in other studies [21] (Fig. 2b).

All simulations are repeated at least 10 times to determine a mean and a standard deviation of ϕ_c. Standard deviations of ϕ_c are about 0.01. The typical number of crystals in each simulation ranges from 10^3 to 3×10^5, depending on particle attributes ξ.

We test our computational method by running simulations for which percolation theory results are well-established [25–28], such as for parallel-aligned cubes, where $\phi_c = 0.29$. Furthermore, we use visualizations of crystal configurations at low crystal numbers to confirm calculations of simulation parameters (Fig. 4).

4. Results

In this section we present our simulation results and reserve interpretation for the discussion section. Fig. 5 shows ϕ_c for biaxial rectangular prisms with aspect ratios ranging from 10^{-2} to 10^2, where 10^0 indicates a cube, and negative and positive exponents indicate oblate and prolate prisms, respectively. All crystals are soft-core objects of uniform size and are oriented randomly. Standard deviations for ϕ_c are shown with vertical bars. A maximum $\phi_c = 0.22 \pm 0.01$ is reached for cubes with decreasing values of ϕ_c for less equant shapes. The dashed curve in Fig. 5 shows results from Garboczi et al. [22] for overlapping, ran-

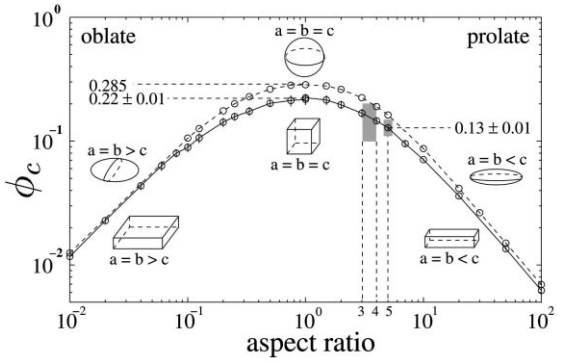

Fig. 5. Simulation results of ϕ_c versus aspect ratio for randomly oriented biaxial soft-core rectangular prisms (solid curve, this study), compared with values for randomly oriented rotational soft-core ellipsoids (dashed curve) determined by [22]. Maximum values of $\phi_c = 0.22 \pm 0.01$ and $\phi_c = 0.285$ are reached for the most equant shapes, i.e. for cubes and spheres, respectively. The number of crystals per simulation ranges from 4×10^2 to 8×10^4 (extreme prolate case). The standard deviation is shown with vertical bars. Two simulations, with 10 repetitions each, are performed for cubes, first with 401 ± 49 cubes and second with 2597 ± 128 cubes. Both simulations yield the same result, indicating that the larger cube size is sufficiently small to avoid finite size effects. The large and small shaded areas represent experimental results from Hoover et al. [10] and Philpotts et al. [2], respectively.

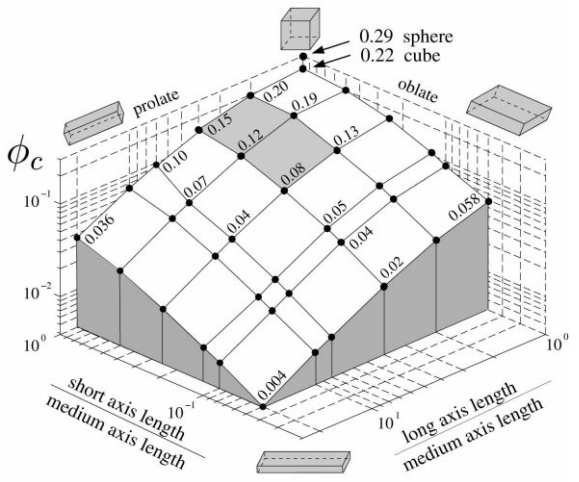

Fig. 6. Simulation results of ϕ_c versus aspect ratio for randomly oriented triaxial soft-core rectangular prisms. A maximum value of $\phi_c = 0.22 \pm 0.01$ is reached for the most equant shape (cube). The gray shaded area indicates the range of aspect ratios for typical tabular plagioclase crystals [2,10,35].

domly placed and randomly oriented, rotational ellipsoids. The general form of the two curves in Fig. 5 is the same, but the curves are offset for the more equant shapes. Both curves converge at the extreme prolate and oblate limits.

Results for triaxial soft-core rectangular prisms at random positions and orientations are shown in Fig. 6. Aspect ratios are given as short over medium and as long over medium axis for oblate and prolate prisms, respectively. Again, the uniaxial limit and thus most equant shape (cube) provides the maximum value of $\phi_c = 0.22 \pm 0.01$. Deviation from an equant shape by either elongation or flattening causes a decrease in ϕ_c, with the largest combined decrease when all three axes have different lengths.

The effect of crystal size on the percolation threshold was examined by simulations involving bimodal size distributions. Fig. 7 shows ϕ_c versus occurrence fraction of large crystals in a bimodal size distribution of soft-core cubes. The volume of a large crystal is $V_{large} = 8V_{small}$, where V_{small} is the volume of a small crystal. For both parallel-aligned (solid line) and randomly oriented (dashed line) crystals, ϕ_c is invariant (to within the stan-

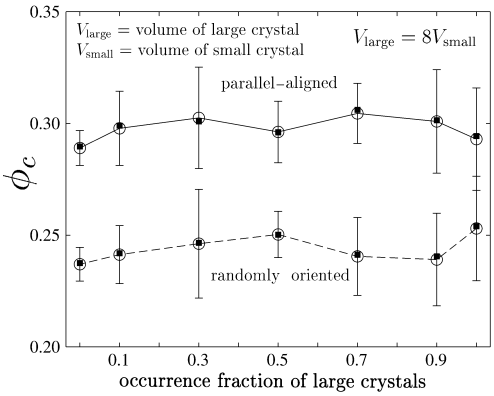

Fig. 7. Critical crystal volume fraction, ϕ_c, versus occurrence fraction of large crystals in a bimodal size distribution. Crystals are parallel-aligned (solid line) and randomly oriented (dashed line) soft-core cubes. Open circles and error bars indicate numerical crystal volume fraction calculations using a space discretization method. Also shown are calculations of crystal volume fraction using the number of crystals, n, and the mean volume of the crystals, V_m, in $\phi = 1 - \exp(-nV_m)$ (filled squares). Error bars for the latter calculation of ϕ are comparable in size to the ones shown.

dard deviation) of bimodal size distribution. Fig. 7 also shows good agreement between calculations of crystal volume fraction using the discretization approach (open circles) and using $\phi = 1 - \exp(-nV_m)$ [23,24], where n is the number and V_m the mean volume of the crystals (solid squares).

5. Discussion

The onset of yield strength, τ_y, can be related to the formation of a continuous particle (or bubble) network that provides some resistance to applied stress [6,16]. This particle network first forms at the percolation threshold, ϕ_c. No yield strength is expected to exist for crystal volume fractions of $\phi < \phi_c$. Transitions in magmatic processes controlled by τ_y may thus not be expected to occur before ϕ has reached or exceeded ϕ_c. Therefore, the percolation threshold, ϕ_c, may be a crucial parameter in understanding the occurrence of transitions in magmatic flow and emplacement behavior.

Guéguen et al. [29] emphasize a necessary distinction between mechanical and transport percolation properties. They suggest that the effective elastic moduli of a material that contains pores and cracks is explained by 'mechanical percolation'. In contrast, elastic moduli for media that contain particles with bond-bending interparticle forces are probably described by the same percolation models that describe transport properties (permeability, conductivity) [29,30]. Therefore, while rheological properties at critical melt fractions [31] probably belong to mechanical percolation that describes solid behavior, the networks of crystals that form solid bonds, investigated in this study, may be a transport percolation problem.

In suspensions, τ_y may be created by friction, lubrication forces, or electrostatic repulsion between individual particles [32]. In addition, crystal–melt suspensions may provide τ_y by solid connections of intergrown crystals. We expect the latter to occur at lower ϕ and provide larger τ_y than friction. Therefore, we consider only the contribution of crystal network formation to τ_y.

5.1. Onset of yield strength

For randomly oriented biaxial soft-core prisms we obtain $0.01 < \phi_c < 0.22$ for oblate crystals with aspect ratios ranging from 0.01 to 1, and $0.006 < \phi_c < 0.22$ for prolate crystals with aspect ratios of 100 to 1, respectively (Fig. 5). Deviation from the uniaxial shape, a sphere for ellipsoids, or a cube for rectangular prisms, leads to a decrease of ϕ_c (Fig. 5). The percolation threshold for spheres and parallel-aligned convex objects of any shape is $\phi_c \approx 0.29$ [25–28]. When anisotropic particles are not perfectly aligned, ϕ_c depends on the orientation distribution of the objects [33,34]. Randomly oriented cubes yield $\phi_c = 0.22 \pm 0.01$ in our simulations, a result that supports the predictions of Balberg et al. [33,34]. Thus, the onset of yield strength is a function of both shape (Fig. 5) and the degree of randomness in the particle orientation, with τ_y occurring at lower ϕ for more elongated or flattened shapes, as well as for more randomly oriented objects. While it is well-established that size heterogeneity of non-overlapping particles, for example in sediments, increases the maximum packing fraction, size heterogeneity of overlapping objects does not appear to influence ϕ_c, as shown in Fig. 7. Therefore, onset of yield strength should not change with size variations of crystals.

Philpotts et al. [2,20] observe a crystal network in the Holyoke flood basalt at total crystal volume fractions of about 0.25. Based on 3D imaging of the crystals using CT scan data, they conclude that plagioclase (aspect ratio 5:1) forms the crystal network, although it comprises only half of the total crystal volume fraction (≈ 0.13). Our results show that the formation of a continuous network of randomly oriented plagioclase crystals of aspect ratio 5:1 at $\phi_c \approx 0.13$ is expected on a purely geometrical basis and thus show good agreement with the experimental results (dashed line at aspect ratio 5 in Fig. 5). Because the elongated plagioclase crystals form a network at lower ϕ_c than the more equant (cube-like) pyroxenes, it may be reasonable, as a first approximation, to model crystal network formation in this plagioclase–pyroxene system with plagioclase crystals only.

Typical plagioclase shapes may be approximated as triaxial polyhedra that are elongated and flattened (tablets). Fig. 6 shows that, for random orientations, the combined effect of three independent axis lengths in rectangular prisms reduces ϕ_c further with respect to biaxial prisms. The shaded area in Fig. 6 indicates the range of rectangular prism shapes that best approximate typical plagioclase crystals [2,10,35]. These plagioclase tablets of aspect ratios (short:medium:long) 1:4:16 to 1:1:2 yield $0.08 < \phi_c < 0.20$, respectively, in our simulations. Therefore, under the condition of random crystal orientation, i.e. in a zero-shear environment, we expect typical plagioclase tablets to form a first fragile crystal network at crystal volume fractions as low as 0.08–0.20, where the particular values depend on the crystal aspect ratios.

Our results also agree reasonably well with Hoover et al.'s [10] analog experiments with prismatic fibers in corn syrup, in which $0.10 < \phi_c < 0.20$ for aspect ratios 3–4 (gray shaded area in Fig. 5). However, the particles in the experiment are non-overlapping, not soft-core as in our simulations, and thus we expect some deviation from the numerical results. In the same study, Hoover et al. [10] conduct partial melting experiments with pahoehoe and 'a'a samples from Hawaii and Lava Butte, OR, USA, respectively. Partially melted pahoehoe samples with subequal amounts of plagioclase and pyroxene show some finite yield strength, and thus the sample maintains its cubical shape, at volume fractions of 0.35 at a temperature of 1155°C. At 1160°C and volume fractions of 0.18, the sample collapses, indicating that the yield strength dropped below the total stress of about 5×10^2 Pa applied by gravitational forces. Backscattered electron images indicate that plagioclase and pyroxene form local clusters and a sample-spanning cluster network at 1155°C (Fig. 8). Cluster formation suggests that crystal configurations in the pahoehoe sample may be dominated by nucleation site effects, possibly due to rapid cooling [36]. If we take the average of the reported median plagioclase aspect ratio of about 1:2:5 and the estimated median pyroxene aspect ratio of 1:1:2, we obtain an aspect ratio of about 1:1.5:3.5 (volume fractions are about equal). For this aspect ratio and random orientation, neglecting clustering effects visible in the experiments, our simulations suggest $\phi_c \approx 0.18$ (Fig. 6).

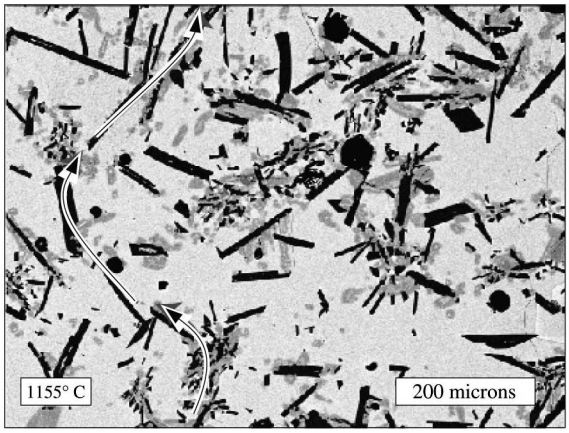

Fig. 8. Backscattered electron image of a pahoehoe sample from Hawaii close to the percolation threshold after partial melting experiments [10]. An image-spanning crystal pathway (arrows) formed of plagioclase (black) and pyroxene (gray) crystals can be observed.

Hoover et al. [10] also carried out melting experiments with 'a'a samples from Lava Butte, OR, USA, containing mainly plagioclase, with only minor pyroxene (volume fraction < 0.05). The plagioclase crystals show some local alignment and exhibit a small τ_y for a plagioclase volume fraction of 0.31 at 1142°C, where the sample shape is preserved, but not at 0.26 at 1150°C, where the sample collapses. The plagioclase aspect ratio is about 1:2:5 for which our simulations suggest $\phi_c \approx 0.16$. However, as discussed above, alignment of crystals causes an increase of ϕ_c, where the upper bound $\phi_c = 0.29$ is reached for parallel-aligned objects of any convex shape.

The general trend of our simulations and other percolation threshold studies appears to be consistent with experiments presented by Hoover et al. [10] and agrees well with experiments presented by Philpotts et al. [2,10] (Fig. 5). The drastic decrease in ϕ_c we observe with increasing particle shape anisotropy and increasing randomness in particle orientation is consistent with other numerical, experimental, and theoretical studies [23,29,37–39] that investigate the formation of continuous object networks.

5.2. Scaling relation for $\tau_y(\phi)$ curves of differing particle shapes, and other generalizations

To develop general rules that explain the dependence of the geometrical percolation threshold, p_c, on object geometries we consider two percolation theory concepts. First is the average critical number of bonds per site at p_c, B_c. Second is the excluded volume, v_{ex}, which is defined as the volume around an object in which the center of another such object cannot be placed without overlap. If the objects have an orientation or size distribution, the average excluded volume of an object is averaged over these distributions and denoted by $\langle v_{ex}\rangle$ and the average critical total excluded volume is given by $\langle V_{ex}\rangle = n_c\langle v_{ex}\rangle$ [33], where n_c is the number of soft-core particles at the percolation threshold. Balberg et al. [33] found that B_c is equal to $\langle V_{ex}\rangle$, i.e.:

$$B_c = n_c\langle v_{ex}\rangle = \langle V_{ex}\rangle \quad (5)$$

and suggested that $\langle V_{ex}\rangle$ is invariant for a given shape and orientation distribution and thus independent of size distribution [34]. Values of $\langle V_{ex}\rangle$ are highest for spheres and parallel-aligned convex objects of any shape, where $\langle V_{ex}\rangle = 2.8$, lowest for orthogonally aligned (macroscopically isotropic) widthless sticks, where $\langle V_{ex}\rangle = 0.7$, and intermediate for randomly oriented cylinders, for which $\langle V_{ex}\rangle = 1.4$ [34]. In natural systems particles can be oriented between random and parallel, depending on the shear stress tensor and particle shapes [9,40], and thus we expect $\langle V_{ex}\rangle$ to fall within the bounds of 1.4 and 2.8. Therefore, $\langle V_{ex}\rangle$ probably varies by a factor of 2 in natural systems.

Shante and Kirkpatrick [25] found $p_c = 1-\exp(-B_c/8)$ for parallel-aligned convex objects in continuum percolation. Using Eq. 5 and $\langle v_{ex}\rangle = 8v$ for spheres (and parallel-aligned convex objects in general), where v is the volume of the sphere, it is possible to make further generalizations. At the percolation threshold, where $n = n_c$, $B = B_c$, and $\phi = p_c$, Eq. 5 is substituted into $\phi = 1-\exp(-nv)$ [23,24] to yield:

$$p_c = 1-\exp(-B_c v/\langle v_{ex}\rangle) \quad (6)$$

for systems containing interpenetrating objects of any convex shape. Eq. 6 and $B_c = \langle V_{ex}\rangle = 2.8$ for spheres agree well with the established percolation threshold $p_c = 0.29$ for soft-core spheres [27]. Soft-core parallel-aligned convex shapes also yield $p_c = 0.29$ [28]. Because the ratio of $v/\langle v_{ex}\rangle$ is constant for objects of different sizes and identical shape and orientation distributions, p_c may be expected to be invariant if only the size distribution changes. This expectation is confirmed in our simulations (Fig. 7).

Generalization of a relationship between p_c, $\langle V_{ex}\rangle$, n_c, and v to include variations in object shapes have been less successful. Garbozci et al. [22] investigate a number of possible shape functionals for randomly oriented soft-core rotational ellipsoids, including $\langle V_{ex}\rangle$. They find that $n_c\langle v_{ex}\rangle \approx 1.5$ and 3.0 for extremely prolate and oblate rotational ellipsoids, respectively, which agrees reasonably well with the range of 1.4 (randomly oriented widthless sticks) to 2.8 (spheres) suggested by Balberg [34]. Similar results for the other shape functionals lead Garboczi et al. [22] to conclude that simple shape functionals do not produce invariants and thus cannot predict p_c for overlapping rotational ellipsoids.

Drory [41] also concluded that the total average excluded volume is not truly universal, but is influenced instead by the shape of objects "in a complicated way". However, Drory et al. [42] point out that $\langle V_{ex}\rangle$ "seemed to be relatively insensitive to the shape of particles" when compared with p_c and that "it was therefore considered an approximately universal quantity". A more rigorous theoretical model is developed to explain values of $B_c = \langle V_{ex}\rangle$ for interacting objects of different shapes [41–43]. While this theory predicts B_c well it does not provide an alternative to B_c that would be a true invariant.

Based on the above studies, we have to content ourselves with $\langle V_{ex}\rangle$ as an approximate invariant that varies by a factor of 2. Predictions of ϕ_c to within a factor of 2 should thus be possible for a large range of particle shapes [38]. In geological applications, a factor of 2 uncertainty in ϕ_c may be too large to interpret some observations, but may still be a valuable constraint for developing models and predictions.

For the case of randomly oriented rods with hemispherical caps of length $L+W$ and width W [33]:

$$\langle v_{ex}\rangle = (4\pi/3)W^3 + 2\pi W^2 L + (\pi/2)WL^2 \quad (7)$$

For $L \gg W$, Eq. 7 reduces to that of Onsager [44]:

$$\langle v_{ex}\rangle \approx (\pi/2)WL^2 \quad (8)$$

Because the calculation of an average excluded volume for randomly oriented rectangular prisms is difficult, we define a volume $v^* = (4/3)\pi r_1 r_2^2$ that scales in a similar manner to Eq. 8. Here, r_1 is the distance from the center to the closest edge and r_2 is the distance to a vertex (Fig. 9). When we normalize v^* by the critical number of crystals per unit volume, n_c, we obtain a quasi-invariant, $n_c v^*$. Between the asymptotic limits of large and small aspect ratios $n_c v^*$ varies by about a factor of 3 (Fig. 9). The relatively small variations of $n_c v^*$ compared with ϕ_c suggests that $n_c v^*$ may be considered a reasonable estimate of a characteristic normalized volume.

If $n\langle v_{ex}\rangle$ were truly invariant, and could be applied to conditions of $\phi \neq \phi_c$ and non-overlapping (hard-core) particles, we could relate the volume fraction for particles of general shape and volume, V, to the volume fraction, ϕ_{eq}, of an equivalent

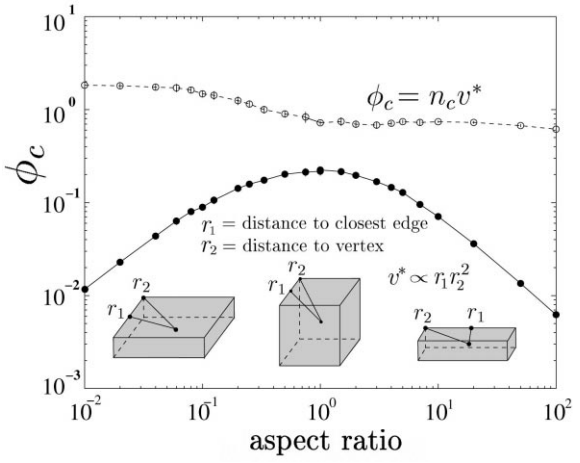

Fig. 9. The volume $v^* = (4/3)\pi r_1 r_2^2$ scales in a similar manner to the average excluded volume (Eq. 8). We normalize v^* by the number of particles, n_c, at the percolation threshold.

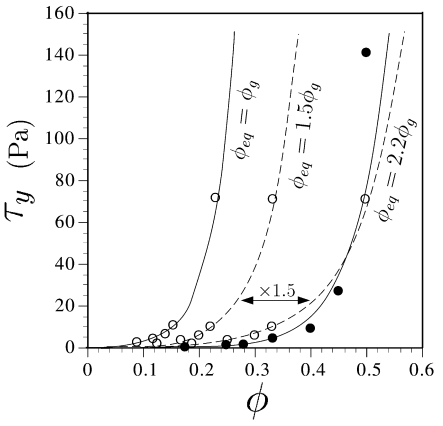

Fig. 10. Scaling of an experimental $\tau_y(\phi)$ curve for fibers of aspect ratio 3.4:1 (open symbols along solid line) to the experimental $\tau_y(\phi)$ curve for spheres (filled symbols); data are from [10]. Dashed lines indicate scaled curves for the fibers using the scaling constants 1.5 and 2.2.

object (here a sphere) by:

$$\phi_{eq} = \frac{\phi_g \langle v_{ex}\rangle_g}{8V_g} \quad (9)$$

where the subscript g denotes values for general particle shapes. For Eq. 9, we use $\phi = nV$ (for hard-core particles). Similarly, for soft-core particles, where $\phi = 1-\exp(-nV)$, we obtain the relationship:

$$\phi_{eq} = 1-(1-\phi_g)^{(\langle v_{ex}\rangle_g/8V_g)} \quad (10)$$

Because $n_c\langle v_{ex}\rangle$ varies by a factor of about 2, scaling in Eqs. 9 and 10 is accurate to a factor of about 2.

As an example, we use Eqs. 7 and 9, and $L = 2.5W$ for hard-core fibers of mean aspect ratio 3.4:1 [10] to calculate that $\phi_{eq} = 1.5\phi_g$. We may then use this scaling constant of 1.5 to scale experimentally measured $\tau_y(\phi)$ curves for these fibers to the values of the equivalent object (sphere). The two curves shown in Fig. 10 can be superimposed using $\phi_{eq} = 2.2\phi_g$. The factor 2.2 is greater than our estimated value of 1.5 by a factor of 1.5, and within the anticipated uncertainty range of a factor of 2.

An equivalent way of interpreting the experimental results is to determine the average ex-

cluded volume, $\langle v_{ex} \rangle$. Our result of $\phi_{eq} = 1.5\phi_g$ implies that $\langle v_{ex} \rangle = 12V_g$ for the hard-core fibers. We now use $\langle v_{ex} \rangle = 12V_g$ together with the computed number of crystals at the percolation threshold, n_c. For biaxial randomly oriented prisms of aspect ratio 3:1 and a normalized particle volume of 1.7×10^{-6}, simulations yield $n_c = 113 \times 10^3$ which results in $n_c \langle v_{ex} \rangle = 2.3$. The average total excluded volume thus falls within the expected range of 1.4 to 2.8 for particle shape and orientation distributions in natural systems.

5.3. Implications

Possible implications of the development of yield strength in crystal–melt suspensions include transitions in surface textures of basaltic lava flows [1], melt extraction from crystal mushes [2], transitions from effusive to explosive volcanism [3], and propagation of shear waves through zones of partial melting [45]. Furthermore, the characteristics of mineral textures and the spatial distribution of ore deposits in komatiites are sometimes explained by fluid dynamical models that suggest post-emplacement convection [46,47]. Aggregate and network formation of dendritic olivine crystals in komatiites increase viscosity and may provide yield strength, which would reduce the convective vigour and may potentially suppress convection. In general, the development of yield strength is likely to affect convective processes in a variety of geologic settings including lava lakes, flood basalts, and magma chambers. Finally, loss of a rigid crystal framework may be a necessary condition for some geologic processes to occur. For example, diapiric ascent of magma through the crust [48] or thorough mixing of partially solidified material into an intruding melt [49] may require loss of continuous crystal networks.

6. Conclusions

We employ numerical simulations for soft-core (overlapping) rectangular prisms to determine the critical crystal volume fraction, ϕ_c, at which a suspension may develop a finite yield strength, τ_y. Our results indicate that ϕ_c is a function of both shape and the degree of randomness in particle orientations. In general, the onset of τ_y should occur at lower crystal volume fractions for larger shape anisotropy, as well as for more randomly oriented objects.

Formation of a sample-spanning network of randomly oriented plagioclase crystals of aspect ratio 5:1 is expected at $\phi_c \approx 0.13$ and thus confirms experimental observations [2,20]. In general, under random orientations, for typical plagioclase aspect ratios ranging from 1:4:16 to 1:1:2 we expect $0.08 < \phi_c < 0.20$, respectively. Randomly oriented crystals that have larger aspect ratios may exhibit yield strength at even lower crystal volume fractions. Therefore, the development of yield strength may occur at lower crystal volume fractions than the 0.35–0.5 commonly assumed [6–8], provided the crystals are anisotropic in shape and exhibit random orientations, as can be the case in low-shear environments.

For overlapping (soft-core) particles, ϕ_c increases with the degree of alignment and reaches a maximum of $\phi_c = 0.29$, the value for spheres, for parallel-aligned particles of any convex shape. This dependence of ϕ_c on the particle orientation distribution suggests that the flow regime, and therefore the resulting particle ordering, of a suspension is an important parameter in defining ϕ_c and hence the onset of yield strength. In contrast, crystal size distributions are not expected to influence ϕ_c unless crystal overlap is inhibited. The presented results of ϕ_c in a zero-shear environment may be viewed as a lower bound for the onset of yield strength in shear environments.

Phenocryst volume fractions larger than 0.30 [50] and even 0.50 [15] have been reported for dikes. Our results suggest that a first minimum yield strength ($\tau_y \to 0$) may develop at much lower volume fractions and potentially impede magma flow. Suppression of flow under high-shear stresses, however, requires ϕ larger than about 0.5 [51]. Thus, it should be emphasized that even for $\phi > \phi_c$, flow can occur if stresses exceed the yield strength.

Finally, we confirm that the average total excluded volume $n\langle v_{ex} \rangle$ is a quasi-invariant that varies by only a factor of about 2 over a large

range of shapes and we suggest that it provides a reasonable means to define an equivalent volume fraction, ϕ_{eq}. ϕ_{eq} captures the characteristic particle geometry that determines onset of ϕ_c and may also be applied to $\phi \neq \phi_c$. Using ϕ_{eq} for all ϕ appears to allow scaling of experimental $\tau_y(\phi)$ curves [10] for suspensions of different particle shapes to within a factor of 2.

Acknowledgements

This work was supported by NSF (EAR 0003303 and EAR 9902851), and a GSA student research grant. Acknowledgement is made to the Donors of the Petroleum Research Fund, administered by the American Chemical Society, for partial support of this research. We also thank John Conery and Wolfram Arnold for computational advice and Bruce Marsh, Ross Kerr, and Jean Vigneresse for their comments and careful reviews of the manuscript. James Kauahikaua and the Hawaiian Volcano Observatory are thanked for their support. *[SK]*

References

[1] K.V. Cashman, C. Thornber, J.P. Kauahikaua, Cooling and crystallization of lava in open channels, and the transition of pahoehoe lava to 'a'a, Bull. Volcanol. 61 (1999) 306–323.

[2] A.R. Philpotts, J. Shi, C. Brustman, Role of plagioclase crystal chains in the differentiation of partly crystallized basaltic magma, Nature 395 (1998) 343–346.

[3] D.B. Dingwell, Volcanic dilemma: flow or blow?, Science 273 (1996) 1054–1055.

[4] F.J. Ryerson, H.C. Weed, A.J. Piwinskii, Rheology of subliquidus magmas, 1: picritic compositions, J. Geophys. Res. 93 (1988) 3421–3436.

[5] D.J. Stein, F.J. Spera, Rheology and microstructure of magmatic emulsions: theory and experiments, J. Volcanol. Geotherm. Res. 49 (1992) 157–174.

[6] R.C. Kerr, J.R. Lister, The effects of shape on crystal settling and on the rheology of magmas, J. Geol. 99 (1991) 457–467.

[7] H. Pinkerton, R.J. Stevenson, Methods of determining the rheological properties of magmas at sub-liquidus temperatures, J. Volcanol. Geotherm. Res. 56 (1992) 108–120.

[8] A.-M. Lejeune, P. Richet, Rheology of crystal-bearing silicate melts: an experimental study at high viscosities, J. Geophys. Res. 100 (1995) 4215–4229.

[9] M. Manga, Orientation distribution of microlites in obsidian, J. Volcanol. Geotherm. Res. 86 (1998) 107–115.

[10] S. Hoover, K.V. Cashman, M. Manga, The yield strength of subliquidus basalts: experimental results, J. Volcanol. Geotherm. Res. (2001), in press.

[11] A. Einstein, Eine neue Bestimmung der Moleküldimensionen, Ann. Phys. 19 (1906) 289–306; English translation in: Investigation on the Theory of Brownian Motion, Dover, New York, 1956.

[12] R. Roscoe, Suspensions, in: J.J. Hermans (Ed.), Flow Properties of Disperse Systems, North Holland, Amsterdam, 1953, pp. 1–38.

[13] H.R. Shaw, Comments on viscosity, crystal settling, and convection in granitic magmas, Am. J. Sci. 263 (1965) 120–152.

[14] D.J. Jeffrey, A. Acrivos, The rheological properties of suspensions of rigid particles, AIChE J. 22 (1976) 417–432.

[15] B. Marsh, On the crystallinity, probability of occurence, and rheology of lava and magma, Contrib. Mineral. Petrol. 78 (1981) 85–98.

[16] Z.Q. Zhou, F. Tunman, G. Luo, P.H.T. Uhlherr, Yield stress and maximum packing fraction of concentrated suspensions, Rheol. Acta 34 (1995) 544–561.

[17] C.R. Wildemuth, M.C. Williams, Viscosity of suspensions modeled with a shear-dependent maximum packing fraction, Rheol. Acta 23 (1984) 627–635.

[18] C.R. Wildemuth, M.C. Williams, A new interpretation of viscosity and yield stress in dense slurries: coal and other irregular particles, Rheol. Acta 24 (1985) 75–91.

[19] H.A. Barnes, K. Walters, The yield strength myth, Rheol. Acta 24 (1985) 323–326.

[20] A.R. Philpotts, L.D. Dickson, The formation of plagioclase chains during convective transfer in basaltic magma, Nature 406 (2000) 59–61.

[21] D. Stauffer, A. Aharony, Introduction to Percolation Theory, Taylor and Francis, London, 1992.

[22] E.J. Garboczi, K.A. Snyder, J.F. Douglas, M.F. Thorpe, Geometrical percolation threshold of overlapping ellipsoids, Phys. Rev. E 52 (1995) 819–828.

[23] I. Balberg, Excluded-volume explanation of Archie's law, Phys. Rev. B 33 (1986) 3618–3620.

[24] E.J. Garboczi, M.F. Thorpe, M. De Vries, A.R. Day, Universal conductivity curve for a plane containing random holes, Phys. Rev. A 43 (1991) 6473–6482.

[25] K.S. Shante, S. Kirkpatrick, An introduction to percolation theory, Adv. Phys. 20 (1971) 325–367.

[26] A.S. Skal, B.I. Shklovskii, Influence of the impurity concentration on the hopping conduction in semiconductors, Sov. Phys. Semicond. 7 (1974) 1058–1061.

[27] G.E. Pike, C.H. Seager, Percolation and conductivity: a computer study. I, Phys. Rev. B 10 (1974) 1421–1434.

[28] S.W. Haan, R. Zwanzig, Series expansion in a continuum percolation problem, J. Phys. A 10 (1977) 1547–1555.

[29] Y. Guéguen, T. Chelidze, M. Le Ravalec, Microstructures, percolation thresholds, and rock physical properties, Tectonophys. 279 (1997) 23–35.

[30] M. Sahimi, S. Arabi, Mechanics of disorderd solids, II, Phys. Rev. B 47 (1993) 703–712.
[31] J. Renner, B. Evans, G. Hirth, On the rheologically critical melt fraction, Earth Planet. Sci. Lett. 181 (2000) 585–594.
[32] R.G. Larson, The Structure and Rheology of Complex Fluids, Oxford University Press, Oxford, 1999.
[33] I. Balberg, C.H. Anderson, S. Alexander, N. Wagner, Excluded volume and its relation to the onset of percolation, Phys. Rev. B 30 (1984) 3933–3943.
[34] I. Balberg, 'Universal' percolation-threshold limits in the continuum, Phys. Rev. B 31 (1985) 4053–4055.
[35] T.L. Wright, R.T. Okamura, Cooling and Crystallization of Tholeiitic Basalt, 1965 Makaopuhi Lava Lake, Hawaii, US Geological Survey Prof. Paper 1004, 1977.
[36] L. Keszthelyi, R. Denlinger, The initial cooling of pahoehoe flow lobes, Bull. Volcanol. 58 (1996) 5–18.
[37] S.H. Munson-McGee, Estimation of the critical concentration in an anisotropic percolation network, Phys. Rev. B 43 (1991) 3331–3336.
[38] A. Celzard, E. McRae, C. Deleuze, M. Dufort, G. Furdin, J.F. Marêché, Critical concentration in percolating systems containing a high-aspect-ratio filler, Phys. Rev. B 53 (1996) 6209–6214.
[39] M.O. Saar, M. Manga, Permeability–porosity relationship in vesicular basalts, Geophys. Res. Lett. 26 (1999) 111–114.
[40] Y. Wada, Magma flow directions inferred from preferred orientations of phenocrysts in a composite feeder dike, Mikaye-Jima, Japan, J. Volcanol. Geotherm. Res. 49 (1992) 119–126.
[41] A. Drory, Theory of continuum percolation. I. General formalism, Phys. Rev. E 54 (1996) 5992–6002.
[42] A. Drory, B. Berkowitz, G. Parisi, I. Balberg, Theory of continuum percolation. III. Low-density expansion, Phys. Rev. E 56 (1997) 1379–1395.
[43] A. Drory, Theory of continuum percolation. II. Mean field theory, Phys. Rev. E 54 (1996) 6003–6013.
[44] L. Onsager, The effects of shapes on the interactions of colloidal particles, Ann. N.Y. Acad. Sci. 51 (1949) 627–659.
[45] G.A. Barth, M.C. Kleinrock, R.T. Helz, The magma body at Kilauea Iki lava lake: potential insights into mid-ocean ridge magma chambers, J. Geophys. Res. 99 (1994) 7199–7217.
[46] H.E. Huppert, R.S.J. Sparks, J.S. Turner, N.T. Arndt, Emplacement and cooling of komatiite lavas, Nature 309 (1984) 19–22.
[47] J.S. Turner, H.E. Huppert, R.S.J. Sparks, Komatiites II: experimental and theoretical investigations of post-emplacement cooling and crystallization, J. Petrol. 27 (1986) 397–437.
[48] B.D. Marsh, On the mechanism of igneous diapirism, stoping, and zone melting, Am. J. Sci. 282 (1982) 808–855.
[49] M.D. Murphy, R.S.J. Sparks, J. Barclay, M.R. Carroll, T.S. Brewer, Remobilization of andesite magma by intrusion of mafic magma at the Soufriere Hills volcano, Montserrat, West Indies, J. Petrol. 41 (2000) 21–42.
[50] Y. Wada, On the relationship between dike width and magma viscosity, J. Geophys. Res. 99 (1994) 17,743–17,755.
[51] R.C. Kerr, J.R. Lister, Comment on "On the relationship between dike width and magma viscosity" by Yutaka Wada, J. Geophys. Res. 100 (1995) 15541.